

FARZANEH VEISI¹, MOHAMMAD ALI ZAZOULI², MOHAMMAD ALI EBRAHIM ZADEH³
JAMSHID YAZDANI CHARATI⁴, AMIN SHIRALIZADEH DEZFULI⁵

EFFECT OF SUNLIGHT AND ULTRAVIOLET RADIATION ON THE EFFICACY OF Fe-DOPED TITANIUM DIOXIDE (Fe-TiO₂) NANOPARTICLES FOR THE REMOVAL OF FURFURAL FROM AQUEOUS SOLUTIONS

Furfural, chemical compound very harmful to human health and difficult to degrade, is used or generated in many industries, including petrochemical, paper, and oil refining industries. The study evaluates the performance of Fe-TiO₂ nanoparticles for the removal of furfural in the presence of sunlight and UV radiation. Fe-TiO₂ nanoparticles were prepared by the sol-gel method, and the characteristics of the resultant nanoparticles were determined using scanning electron microscopy. Samples with known concentrations of furfural and nanoparticles were individually exposed to sunlight and UV radiation under varying conditions, and the residual furfural concentration was measured using high-performance liquid chromatography. The results showed that for both processes the efficiency of furfural removal increased with increased reaction time, nanoparticle loading, and pH, whereas the efficiency decreased with increased furfural concentration. The highest removal efficiencies of the Fe-TiO₂/UV and Fe-TiO₂/sun processes were 95 and 76%, respectively. In general, the degradation and elimination rate of furfural using Fe-TiO₂/UV process was higher than Fe-TiO₂/sun process because TiO₂ nanoparticles can only be activated upon irradiation with photons of light in the UV domain.

¹Health Sciences Research Center, Student Research Committee, Mazandaran University of Medical Sciences, Sari, Iran.

²Department of Environmental Health Engineering, Health Sciences Research Center, Faculty of Health, Mazandaran University of Medical Sciences, Sari, Iran, corresponding author, e-mail address: zazoli49@yahoo.com

³Department of Pharmaceutical Chemistry, Faculty of Pharmacy, Mazandaran University of Medical Sciences, Sari, Iran.

⁴Department of Biostatistics, Health Sciences Research Center, Faculty of Health, Mazandaran University of Medical Sciences, Sari, Iran.

⁵Faculty of Chemistry, Tehran University, Tehran, Iran.

1. INTRODUCTION

Furfural is produced or used in many industries, such as petrochemical, petroleum refining, pharmaceutical, food, pulp and paper industries [1]. This chemical is used as a solvent for extractive refining of compounds containing oxygen or sulfur such as lubricating oils. Furfural is also a feedstock for the production of furfuryl alcohol, which is used to produce resins and tetrahydrofuran [2]. However, furfural is toxic when inhaled or swallowed, and is harmful upon contact with skin. It can be easily absorbed through the skin and thus cannot be released into bodies of water or sewer systems. Long-term exposure can lead to feelings of weakness, liver enlargement, skin rash, shuddering, nose bleeds, or inflammation, and furfural also shows some limited carcinogenic effects [2, 3].

Advanced oxidation processes (AOPs) are a new technology for the treatment of toxic and polluted water and wastewater [4]. AOPs are based on techniques that normally involve the generation of strong oxidizing species such as hydroxyl radicals ($\cdot\text{OH}$), which oxidize a wide range of pollutants to form less harmful substances, such as water and carbon dioxide [4]. Among the variety of semiconductors available that can be used to generate oxidizing species, titanium dioxide (TiO_2) is the most widely used because it is cost-effective, non-toxic, photochemically stable, widely available, environmentally friendly, insoluble in water, and has a high removal efficiency for pollutants under most environmental conditions [4]. However, the efficiency of TiO_2 is limited by the rate of electron transfer to oxygen, and its large energy band gap of 3.2 eV, corresponding to a wavelength of 370 nm, which leads to the absorption of only 3–5% of solar light. Various methods have been developed to improve the photocatalytic activity of TiO_2 particles, including more efficient particle sizes, higher surface-to-volume ratios, and surface modification with other semiconductor metal ions, such as gold [5], palladium [6], platinum [7], silver [8], and lanthanum [9]. Li et al. [9] used the lanthanum doping TiO_2 ($\text{La}^{3+}\text{-TiO}_2$) photocatalysts for 2-mercapto-benzothiazole (MBT) control. The results showed that both the adsorption capacity and adsorption equilibrium constants of photocatalysts increased with an increase of lanthanum doping. They concluded that the enhancement of MBT photodegradation using the $\text{La}^{3+}\text{-TiO}_2$ photocatalysts mainly involved in both the improvement of the organic substrate adsorption in photocatalysts suspension and the enhancement of the separation of electron-hole pairs owing to the presence of Ti^{3+} . Pearson et al. [10] researched the employment of the Keggin ion 12-phosphotungstic acid as a UV-switchable reducing agent for the decoration of Au, Ag, Pt, and Cu nanoparticles onto the surface of TiO_2 nanotubes. They reported that decoration with metal nanoparticles was observed to enhance the activity of the photocatalytic process by upward of 100% with respect to unmodified TiO_2 nanotubes. Primo et al. [11] recommended that the titania supported gold nanoparticles (Au/TiO_2) can be used as photocatalyst for environmental remediation. Because iron ions, such as Fe(III) with a band-gap energy of 2.2 eV, have high

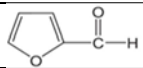
photodegradation efficiency and are less expensive than other semiconductors, Fe(III) was selected as an additive for photodeposition in this study[12]. Previous studies have focused on the removal of furfural using titanium dioxide, however, Fe-doped titanium dioxide nanoparticles have not been investigated for furfural removal. The objective of this study is to investigate the effect of sunlight and ultraviolet radiation on Fe-doped titanium dioxide (Fe-TiO₂) nanoparticles for the removal of furfural from aqueous solution.

2. EXPERIMENTAL

Reagents. This study was performed in a batch system. All chemicals used were analytical grade, obtained from Merck and used without any further purification. The desired pH was obtained using 0.1 M NaOH or 0.1 M H₂SO₄. Double distilled deionized water was used throughout the experiments. The primary characteristics of furfural according to the manufacturer are presented in Table 1.

Table 1

Chemical structure and characteristics of furfural

Chemical structure	
Molecular weight, Da	96.09
Density, g/cm ³	1.159
λ_{\max} , nm	254
pH	5
Solubility in water (20 °C), g/dm ³	83
Color	light brown

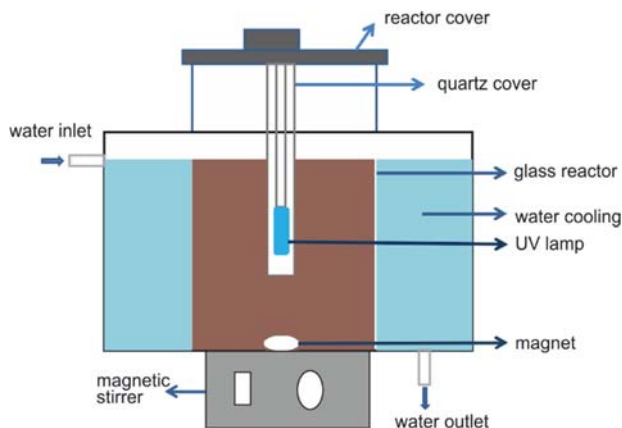


Fig. 1. Schematic of the photoreactor

Photoreactor. The schematic in Fig. 1 shows the reactor used, which is composed of two cells. The exterior Pyrex cell holds the solutions and has a 2.0 dm³ capacity, with a 10 cm inner diameter and 15 cm height. Irradiation experiments were performed using a UVC lamp (125 W) in the inner cell. The lamp was purchased from Arda Co., France. The UV lamp was placed in a 5 cm diameter quartz tube with one end tightly sealed by a Teflon stopper. The lamp and tube were immersed in the photoreactor cell, with a 4.0 cm long light path. A magnetic stirrer was used to ensure thorough mixing of the solutions. To maintain a constant temperature, the reactor was surrounded by 10 dm³ of cooling medium.

Photocatalytic experiments. The experiments were conducted with two irradiation sources; furfural was removed from synthetic solutions using Fe-TiO₂ nanoparticles under UV light, or sunlight. The impact of variables such as furfural concentration, pH, time, and dose of nanoparticles was also investigated.

In the study, the treatment with Fe-TiO₂ nanoparticles in the presence of UV radiation was carried out using nanoparticle concentrations of 125, 250, 625, 1000, and 1375 mg/dm³, furfural concentrations of 25, 50, 125, 200, and 275 mg/dm³, initial pH of 3, 4.5, 6, 7.5, and 9, and contact times of 15, 30, 75, 120, and 165 min.

For the solar process, the contact time was constant and furfural of concentrations of 25, 50, 125, 200, and 251 mg/dm³ was used at pH of 3.4, 4.5, 6, 7.5, and 8.5, and nanoparticle concentrations of 5, 250, 625, 1000, and 1250 mg/dm³. Experiments in the presence of sun were performed in May with an average temperature of 29 °C. The samples were exposed to sunlight from 10 am to 3 pm (5 h) in the area of the Mazandaran University of Medical Sciences, Sari, Iran, which has a latitude and longitude of 48.17° and 38.15°, respectively.

Before being exposed to sunlight or UV radiation, the samples were ultrasonically mixed for 15 min and kept in the dark for 30 min to homogenize the nanoparticles in the solution containing TiO₂. The UV photocatalytic process occurred in the solution closest to the UV lamp and the solution was stirred continuously using a magnetic stirrer. To prevent unwanted exposure to sunlight, all the samples and the reactor were covered with aluminum foil. After completion, the Fe-TiO₂ particles were removed by centrifuging the samples at 4000 rpm for 30 min followed by smooth filtering to 0.45 μm [13].

Analytical methods. The furfural concentration in the samples was analyzed using a high-performance liquid chromatograph (HPLC, Knauer Advanced Scientific Instruments) with a UV absorption detector set at 254 nm. A C₁₈ column was used and the applied mobile phase comprised deionized water and gradient grade acetonitrile at the ratio of 40:60 and flow rate of 1 cm³/min [13].

Synthesis of Fe-TiO₂ nanoparticles. The Fe-TiO₂ nanoparticles were prepared by the sol-gel method. TiCl₄ solution (4.128 cm³, 0.0375 mM) was added to ethanol (70 cm³)

followed by the addition of Fe (NO₃)₃·9H₂O (0.05g in 2 cm³ distilled water). While stirring, propylene oxide (17 cm³) was added dropwise at 50 °C. The gel formed over ca. 5 min; the time required for gel formation depends on the rate of propylene oxide consumption. The resulting gel was aged at room temperature for 48 h and dried for 12 h at 80 °C. To generate the anatase form, the dried gel was calcined for 2 h at 350 °C. The obtained powder was used to perform the tests. Analysis of the prepared Fe-TiO₂ nanoparticles was performed using a scanning electron microscope (Leo 1455 VPSEM) [14].

Experimental design. The central composite design (CCD) model was used to estimate the number of experiments required and investigate the combined effect of the independent variables. In this model for the UV irradiation, four independent variables were pH, catalyst dose, initial concentration, and contact time. For the sunlight irradiation, three independent variables were pH, catalyst dose, and initial concentration. A total of 20 and 31 experiments were introduced for the Fe-TiO₂/sun and Fe-TiO₂/UV processes, respectively. Table 2 shows the ranges and values of the independent variables for the two processes. The range of each variable associated with the model was estimated using the regression formula. Values were obtained using placement-associated codes (2, 1, 0, -1, -2) and (1.68179, 1, 0, -1, -1.68179) for the UV and sunlight methods, respectively.

Table 2

Independent variables, their coded levels and actual values

	Symbol	Variable	Range and level				
			2	1	0	-1	-2
Fe-TiO ₂ /UV	X1	pH	9	7.5	6	4.5	3
	X2	furfural concentration, mg/dm ³	275	200	125	50	25
	X3	catalyst dose, mg/dm ³	1375	1000	625	250	125
	X4	contact time, min	165	120	75	30	15
Fe-TiO ₂ /sun	Symbol	Variable	Range and level				
			1.68179	1	0	-1	-1.68179
	X1	pH	8.5	7.5	6	4.5	3.4
	X2	furfural concentration, mg/dm ³	251	200	125	50	25
	X3	catalyst dose, mg/dm ³	1250	1000	625	250	5

Statistical analysis. A full quadratic model (FQM) was used to assess the obtained data. Optimizations were performed using the Design Expert 16 software. The experiments were conducted randomly to prevent systematic error. The coefficients of the full quadratic model were used to determine the furfural removal rate as an independent variable.

The results were fitted to an empirical quadratic polynomial model to determine the parameters using response surface method (RSM) for both processes, as follows:

$$Y = A_0 + A_1(X_1) - A_2(X_2) + A_3(X_3) + A_4(X_4) - A_5(X_3)^2 - A_6(X_4)^2 \quad (1)$$

where Y denotes the responding variable (furfural removal percent), A_0 is the intercept, A_1 , A_2 , A_3 , and A_4 are the coefficients of the independent variables, A_5 and A_6 are the quadratic coefficients, and X_1 , X_2 , X_3 , and X_4 are terms for the coded values of the independent variables, i.e., pH, furfural initial concentration, catalyst loading, and contact time, respectively. X_3 was used as the catalyst loading parameter for both experiments, and X_4 as the contact time for UV experiments. The data were analyzed using the analysis of variance (ANOVA) and multiple regressions. The amount ($p \leq 0.05$) was set as the level of significance. The ability of the final model was evaluated using numerical and graphical analysis. This statistical model gives the final form of the equation [15].

3. RESULTS AND DISCUSSION

Figure 2a shows a SEM image of the Fe-TiO₂ nanoparticles. The titanium oxide powders have spherical microstructures with an average diameter of 37.89 nm, as determined using the measurement software. Figure 2b shows X-ray diffraction (XRD) patterns of Fe-doped TiO₂ nanoparticles. As the prepared Fe-doped TiO₂ is composed of only anatase, without any presence of iron oxide, regardless of the amount of Fe dopant (less than 12 atomic %). The absence of iron oxide demonstrates that Fe³⁺ ions are successfully incorporated into the framework of the anatase TiO₂, without the formation of iron oxide on the surface of TiO₂. The characteristic peaks for Fe-doped TiO₂, however, are shifted slightly to lower 2θ values. Its incorporation gives rise to the structural expansion of the crystalline lattice, subsequently its structural distortion. The increase in the interplanar distance of the anatase framework causes the XRD peak patterns to shift to a lower 2θ values according to Bragg's law. Thus, the peak shift can be regarded as indirect evidence of successful iron doping into the TiO₂ crystal framework [15]. Figure 3 shows the histogram of the particle size distribution.

Tables 3 and 4 show the results of furfural removal via the Fe-TiO₂/sun and Fe-TiO₂/UV processes, respectively. Irradiation with UV light resulted in the removal of a greater amount of furfural than the irradiation method under varying conditions. Based on data analysis, the correlations between the furfural removal efficiency and parameters for the Fe-TiO₂/UV and Fe-TiO₂/sun methods are represented by Eqs. (2) and (3), respectively.

The efficiency of furfural removal using the Fe-TiO₂/sun is described by:

$$Y = 60.768 + 7.812(X_1) - 4.590(X_2) + 2.733(X_3) - 3.577(X_3)^2 \quad (2)$$

where Y is the percentage removal of furfural and X_1 , X_2 , and X_3 represent the coded values for pH, initial furfural concentration, and catalyst loading, respectively.

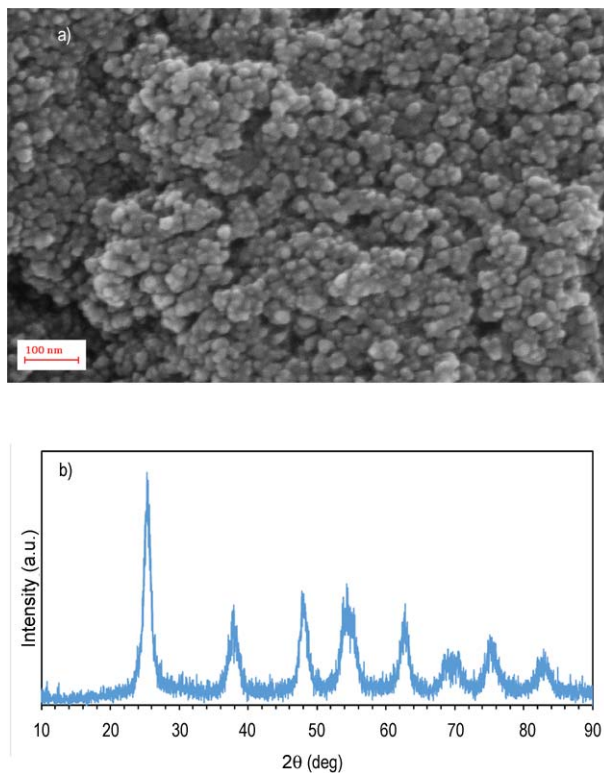


Fig. 2. SEM and XRD images of the prepared Fe-TiO₂ nanoparticles

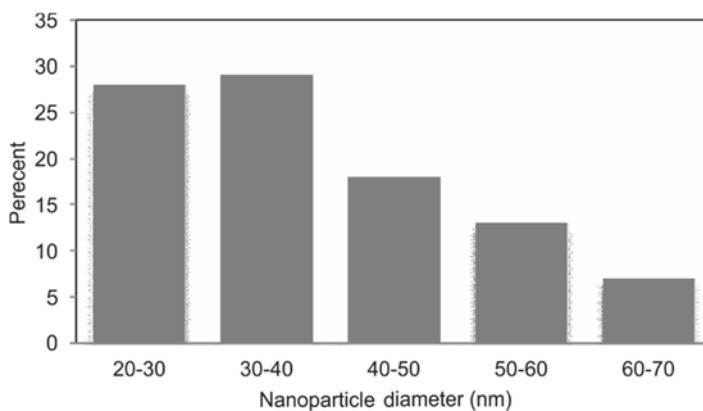


Fig. 3. Histogram showing the Fe-TiO₂ particle size distribution

Table 3

CCD model with predicted and experimental results
for furfural removal using the Fe-TiO₂/sun process

Run	Experimental conditions			Removal [%]	
	pH	Furfural concentration [mg/dm ³]	Catalyst dose [mg/dm ³]	Experimental	Predicted
1	4.5	50	250	57	55.73
2	3.4	125	625	53	52.51
3	6	125	625	62	60.76
4	6	25	625	74	71.36
5	6	125	1250	60	60.76
6	7.5	200	250	70	64.17
7	4.5	200	250	59	63.19
8	7.5	50	250	72	69.85
9	7.5	200	1000	68	67.64
10	4.5	200	250	43	39.05
11	4.5	200	1000	50	50.51
12	6	125	625	60	55.24
13	6	251	625	51	55.93
14	6	125	5	39	46.05
15	8.5	125	625	76	78.78
16	6	125	625	60	60.76
17	7.5	50	1000	67	69.32
18	6	125	625	62	60.76
19	6	125	625	60	60.76
20	6	125	625	61	61.76

Table 4

CCD model with predicted and experimental results
for furfural removal using the Fe-TiO₂/UV process

Run	Experimental conditions				Removal [%]	
	pH	Furfural concentration [mg/dm ³]	Contact time [min]	Catalyst dose [mg/dm ³]	Experimental	Predicted
1	7.5	50	120	1000	95	94.50
2	6	125	75	625	81	80.42
3	6	125	75	625	80	80.42
4	6	125	75	625	82	82.54
5	6	125	75	125	62	61.12
6	4.5	50	120	250	71	74.16
7	6	125	75	625	79	81.62
8	3	125	75	625	65	70.79
9	9	125	75	625	95	90.95
10	4.5	200	30	1000	63	62.00
11	4.5	50	120	1000	82	82.54

Table 4

CCD model with predicted and experimental results
for furfural removal using the Fe-TiO₂/UV process

Run	Experimental conditions				Removal [%]	
	pH	Furfural concentration [mg/dm ³]	Contact time [min]	Catalyst dose [mg/dm ³]	Experimental	Predicted
12	4.5	50	30	1000	78	71.16
13	6	25	75	625	81	80.29
14	6	275	75	625	60	62.45
15	4.5	200	30	250	49	47.50
16	6	125	75	625	80	80.42
17	7.5	50	30	250	63	62.00
18	7.5	200	30	1000	73	67.83
19	7.5	200	30	1000	70	74.87
20	6	125	75	1375	79	81.62
21	6	125	75	625	82	80.42
22	6	125	15	625	37	42.62
23	7.5	200	30	250	56	55.79
24	4.5	200	120	1000	72	74.87
25	4.5	50	30	250	58	56.04
26	7.5	50	120	250	87	88.37
27	4.5	200	120	250	68	63.37
28	7.5	200	120	1000	83	85.20
29	6	125	75	625	81	80.42
30	6	125	75	625	82	82.54
31	7.5	200	120	250	75	79.83

The efficiency of furfural removal by the Fe-TiO₂/UV method is described by:

$$Y = 80.4286 + 5.8750(X1) - 5.2083(X2) + 8.8750(X3) + 5.1250(X4) - 4.9926(X3)^2 - 2.2426(X4)^2 \quad (3)$$

where Y is the percentage removal of furfural and $X1$, $X2$, $X3$, and $X4$ represent the coded values for pH, initial furfural concentration, catalyst loading, and contact time, respectively.

To acquire a suitable model, the results were summarized in a common ANOVA table (Table 5). To confirm the fit between the model and the experimental results, the regression coefficient (R -squared) analysis was applied. The adjusted R -squared values close to 1.0 (minimizing the square of errors) indicate that the regression line fits the experimental data well [16]. This equation can be used to predict the results at specific points with the accuracies of 79.21 and 83.57% for the sun and UV processes, respectively. This model could also be used to predict the percentage of furfural removal at other catalytic contents and times.

Table 5

Analysis of variance for proposed model for furfural removal
by the Fe-TiO₂/sun and Fe-TiO₂/UV methods

Process	Source	Degrees of freedom	Sum of squares	Mean square	<i>F</i> -value	<i>P</i> -Value
Fe-TiO ₂ /sun	regression	9	1591.61	176.845	9.08	0.001
	linear	3	1223.01	407.669	20.84	0.001
	square	3	268.10	89.367	4.57	0.029
	interaction	3	100.50	33.80	1.71	0.227
	residual error	10	195.59	19.559	<i>R</i> -squared	89.06%
	pure error	5	4.83	0.967	Adj. <i>R</i> -squared	79.21%
	total	19	1787.20			
Fe-TiO ₂ /UV	regression	14	4936.58	352.61	11.9	<0.0001
	linear	4	4000.17	1000.04	33.75	<0.0001
	square	4	807.04	201.76	6.81	0.0002
	interaction	6	129.37	21.56	0.73	0.634
	residual error	16	474.13	29.63	<i>R</i> -squared	91.24%
	pure error	6	5.71	0.95	Adj. <i>R</i> -squared	83.57%
	total	30	5410.71			

The adjusted *R*-squared value is a modification of *R*-squared that adjusts for the number of explanatory terms in a model. Unlike *R*-squared, the adjusted *R*-squared value increases only if the new term improves the model more than would be expected by chance. The adjusted *R*-squared value can be negative and will always be less than or equal to *R*-squared. The adjusted *R*-squared value is more suitable for comparing models with different numbers of parameters [16]. The adjusted *R*-squared values for the sun and UV processes are 0.7921 and 0.8357, respectively. Table 5 also shows that the model statistically follows a linear pattern. However, there is significant relation of Fe-TiO₂/sun and Fe-TiO₂/UV with the linear models.

The summary of the results of variance analyses for the Fe-TiO₂/sun and Fe-TiO₂/UV processes are shown in Figs. 4 and 5, respectively. The analysis of the model using ANOVA requires the following assumptions: (1) The residuals have a normal distribution with a zero mean, (2) there is constant variance, and (3) the residuals are independent. If these assumptions are valid, the selected model is adequate to fit the experimental data. Otherwise, an alternative model should be selected and evaluated.

Figures 4a and 5a show normal probability plots of the residuals from the least-squares fitting. The points on the plots lie reasonably close to a straight line, which confirms that the errors have a normal distribution with a zero mean. In addition, the input variables affect the responses. Figures 4b and 5b show random scatter plots of the residuals versus the fitted values. The figures do not reveal an obvious pattern. The predicted results were revealed to be randomly scattered around the zero line (above and below the *x*-axis), which supports the adequacy of the proposed model.

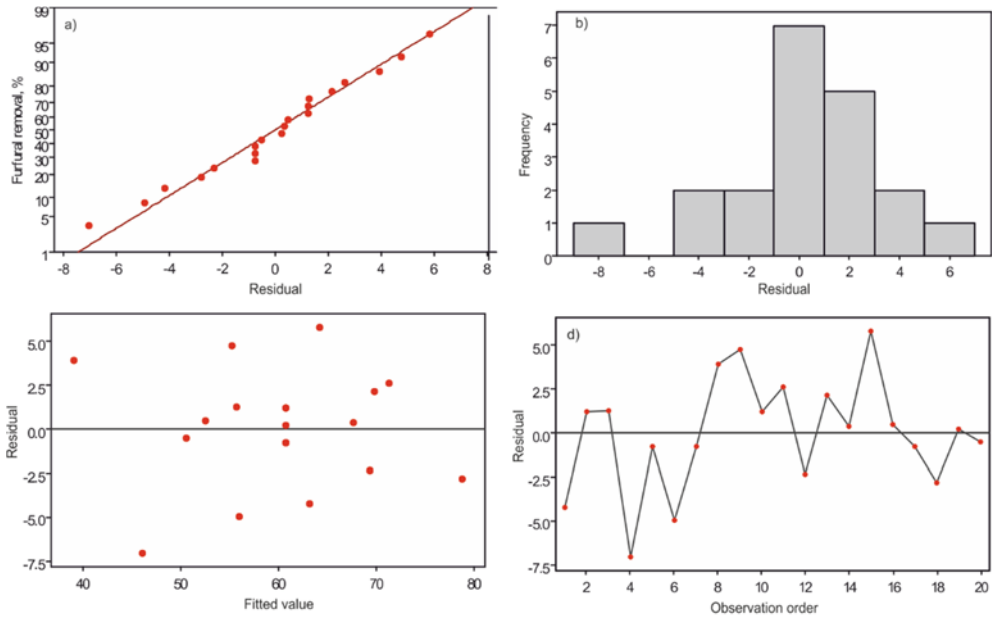


Fig. 4. Residual plots for furfural removal by the Fe-TiO₂/sun process: a) normal probability plot, b) scatter plot, c) histogram, d) versus order

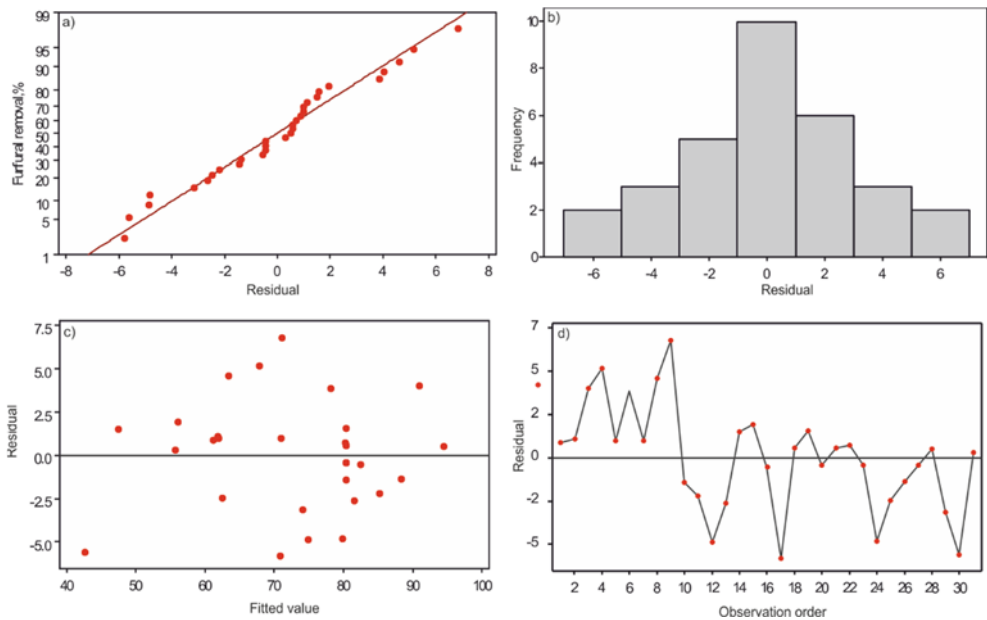


Fig. 5. Residual plots for furfural removal by the Fe-TiO₂/UV process a) normal probability plot, b) scatter plot, c) histogram, d) versus order

Figures 4c and 5c show the frequencies of the residuals, and indicate that there are no outliers in the data. Figures 4d and 5d show that the ordered residuals oscillate in a random pattern around the zero line. Accordingly, the residuals appear to be randomly scattered along the zero line, which indicates that the error terms do not correlate with each other.

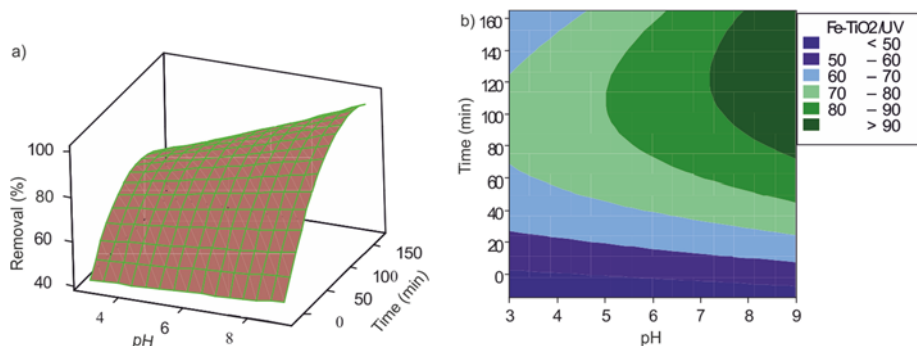


Fig. 6. Surface plot (a) and contour plot (b) of the furfural removal efficiency (%) as a function of reaction time (min) and pH for the Fe-TiO₂/UV process; initial furfural concentration 125 mg/dm³, catalyst loading 625 mg/dm³

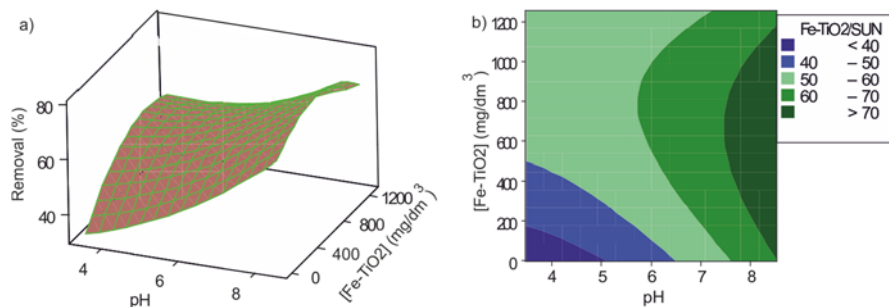


Fig. 7. Surface plot (a) and contour plot (b) of the furfural removal efficiency (%) as a function of catalyst dose (mg/dm³) and pH for the Fe-TiO₂/sun process; initial furfural concentration 125 mg/dm³

Three-dimensional surfaces and contour plots are graphical representations of regression equations for the optimization of reaction conditions. The results of the interactions between the independent variables and the dependent variable for the removal of furfural using nanoparticles are shown in 3D plots and contour plots in the presence of UV and sunlight in Figs. 6 and 7, respectively. It is evident that the removal efficiency increases with increasing contact time and increasing pH. The removal rate of the UV light process was higher than that of the sunlight process.

In the statistical method, all variables are examined at the same time; in order to evaluate the effect of concentration, all other variables should be kept uniform. Runs 10 and 12 in Table 2, for the photocatalytic method with UV, only vary in the concentration of

furfural; the furfural concentrations in runs 10 and 12 are 200 and 50 mg/dm³, respectively. The percent removals of furfural were 63 and 78% for runs 10 and 12, respectively. In all experiments, the efficiency decreased with increasing furfural concentration, because the constant light intensity results in lower number of furfural molecules absorbed the photons. This leads to a reduction the furfural degradation and lower efficiency; the concentration varies linearly, which is in agreement with other studies [16]. As shown in Figs. 8 and 9, furfural removal efficiency decreases with increasing concentration.

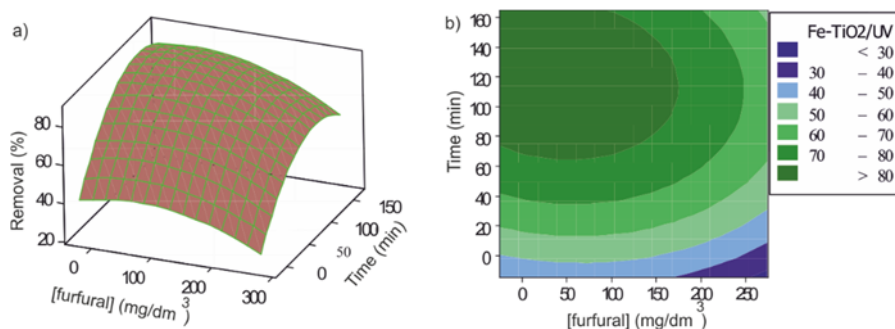


Fig. 8. Surface plot (a) and contour plot (b) of the furfural removal efficiency (%) as a function of reaction time (min) and furfural concentration (mg/dm³) for the Fe-TiO₂/UV process; pH 6, catalyst loading, 625 mg/dm³)

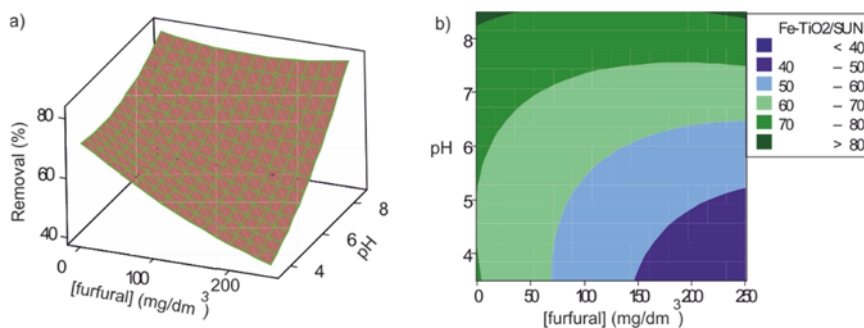


Fig. 9. Surface plot (a) and contour plot (b) of the furfural removal efficiency (%) as a function of furfural concentration (mg/dm³) and pH for the Fe-TiO₂/sun process; catalyst loading 625 mg/dm³)

pH of a solution is one of the most crucial parameters in photocatalytic processes for the degradation and removal of organic contaminants. pH governs the protonation or deprotonation of target compounds in aqueous solutions, thus affecting the efficiency of the photocatalysis process [17]. Figures 6 and 7 show the removal efficiency of furfural at several initial pH using Fe-TiO₂ nanoparticles in the presence of ultraviolet and sun radiation, respectively. The removal efficiency increases with increasing pH. pH of the solution affects the electrostatic force between the catalyst surface and the pollutant. Hydroxyl radical are produced due to irradiation of the catalyst. This radical reacts with

furfural causing furfural degradation and conversion to the final products. The degradation rate of furfural increases with increasing concentration of hydroxyl radicals, and the concentration of hydroxyl ions increases with increasing pH. The pH effect observed in this study agrees with those reported by Chun-Li et al. [14], Sahu et al. [18].

According to Table 3 and Figs. 6 and 7, the relationship between the reaction time and removal of furfural is predominantly linear and positive; the removal efficiency increases with increasing reaction time. However, the chi-square reaction time (is statistically significant and negative. As shown in Figs. 6 and 7, the removal efficiency of furfural did not increase with time over 75 min; thus, the removal efficiency after 75 min was approximately equal to that at 165 min for both processes. The removal efficiency increases with increasing reaction time because the increased time enables more UV irradiation of the nanoparticles. The results of this study agree with those of other studies [13].

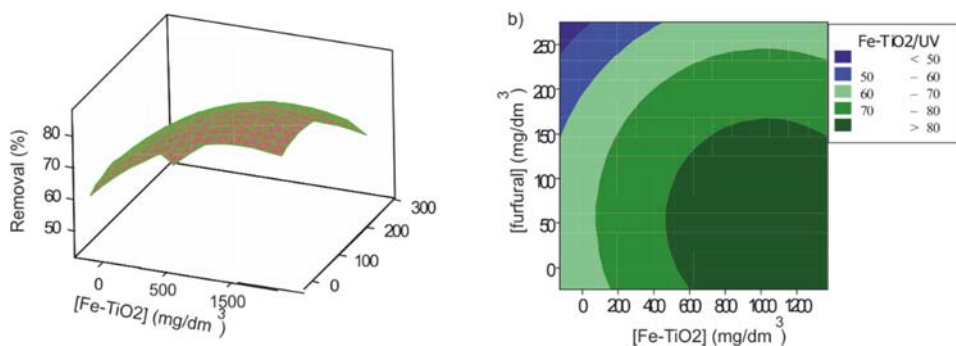


Fig. 10. Surface plot (a) and contour plot (b) of the furfural removal efficiency (%) as a function of Fe-TiO₂ concentration (mg/dm³) and furfural concentration (mg/dm³) for the Fe-TiO₂/UV process; pH 6, 75 min

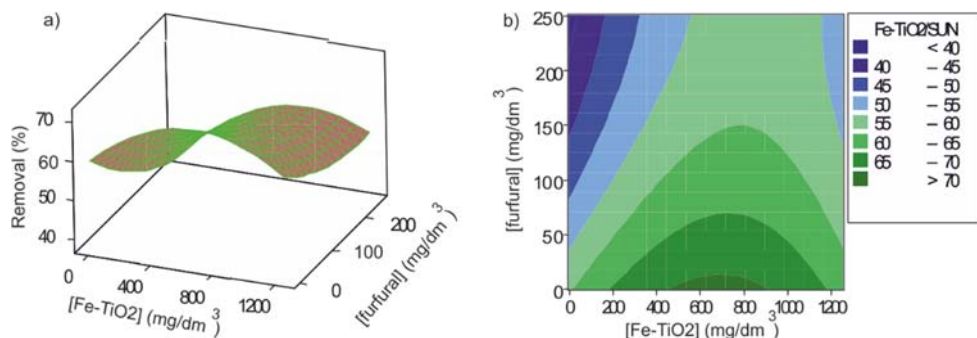


Fig. 11. Surface plot (a) and contour plot (b) of the furfural removal efficiency (%) as a function of the furfural concentration (mg/dm³) and Fe-TiO₂ concentration (mg/dm³) for the Fe-TiO₂/sun process (pH 6)

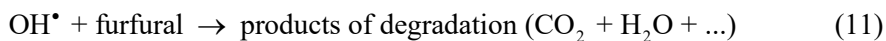
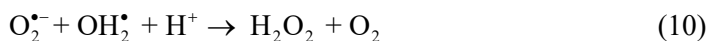
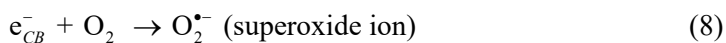
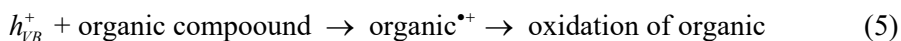
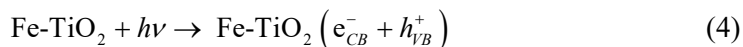
In all experiments, the removal efficiency of furfural increases with increasing nanoparticle dosage. However, at concentrations higher than 1000 mg/dm³, the removal efficiency decreases; this may be due to catalyst aggregation, which reduces the number

of active sites available on the nanoparticle surface, which reduces the quantity of free hydroxyl radicals and hence impairs degradation. Moreover, a high concentration of photocatalyst will result in decreased light penetration through the suspension [19]. This finding is in agreement with literature reports on the effect of catalyst concentration on treatment efficiency [20]. Figures 10 and 11 show that removal efficiency increases with increasing nanoparticle loading. However, if too high a concentration of nanoparticles is used, the removal efficiency decreases.

Tables 3 and 4 show that the highest degradation of furfural in the Fe-TiO₂/UV and Fe-TiO₂/sun processes were 95 and 76%, respectively. The removal efficiency under UV light is more significant than that under sunlight because of the differences in energy of these light sources below 370 nm. The Fe-TiO₂ energy gap is equal to 3.2 eV and, therefore, it can only absorb wavelengths shorter than 370 nm. On the other hand, it can absorb a small amount of solar energy [4]. The TiO₂ nanoparticles have a large band gap and can only be activated by UV radiation. Ultraviolet light makes up only 4–5% of the solar spectrum, whereas approximately 40% of solar photons are in the visible region. It is mean that TiO₂ nanoparticles can only be activated upon irradiation with photons of light in the UV domain, limiting the practical efficiency for solar applications [21]. Therefore, in order to enhance the efficiency of TiO₂ under solar irradiation, it is necessary to dope the TiO₂ to facilitate visible light absorption. In any case; in the presence of sunlight, the band gap of TiO₂ decreases because the interaction of highly reactive electrons with air molecules is expected to give rise to highly reactive and strong oxidizing agents such as OH groups or other radicals, which can react further with TiO₂ nanoparticles. The interaction of TiO₂ with the high energy electrons generated by sunlight and oxidizing agents can result in the reduction of Ti⁴⁺ to Ti³⁺, or the formation of oxygen deficient/rich species [22]. Moreover, the solar experiments were performed in Sari County (north of Iran) in indirect sunlight; these factors contributed to reducing the photocatalytic efficiency in the presence of sunlight. If these experiments were performed in southern cities in Iran where the sun shines more directly, the removal efficiency might increase. The study conducted by Zazouli et al. [23] showed that TiO₂ in the presence of sunlight has very low efficiency due to its energy gap and the corresponding absorbance wavelength. They showed that the highest degradation efficiency of TiO₂/UV and TiO₂/sun (non-doped TiO₂) methods were 87% and 45%, respectively. Whereas in this study, it was observed that the degradation of furfural using Fe-TiO₂/UV and Fe-TiO₂/sun were 97% and 76%, respectively. In other words, the efficiency of Fe-TiO₂ nanoparticles was higher than that of non-doped TiO₂ nanoparticles.

Absorption of a photon with energy equal to or greater than the band gap of a material, such as the Fe-TiO₂ catalyst, results in excitation of electrons from the valence band to the conduction band to form positive holes in the valence band. The generated electrons and holes are quickly distributed in the bottom layer and top layer conduction bands, respectively, according to their kinetic energy. The electrons and holes are then

available for redox reactions. The photocatalytic activity of Fe-TiO₂ depends on competition between the rate of transferring surface charge carriers and the recombination rate of electrons and holes [24, 25].



The photocatalytic degradation of furfural with Fe-TiO₂ proceeds as follows [26]. The holes and electrons are generated on the surface of the catalyst under irradiation (Eq. (4)). Direct oxidation of organic compound can also occur due to an oxidative generated hole in the catalyst (h_{VB}^+) (Eq. (5)). Hydroxyl radicals can be formed either by decomposition of water (Eq. (6)) or the reaction of hole with OH⁻ [Eq. (7)]. Electron in the conduction band (e_{CB}^-) can reduce molecular oxygen to a superoxide anion (Eq. (8)). This radical may form organic peroxide or hydrogen peroxide (Eqs. (9) and (10)). The hydroxyl radicals are the primary sources of degradation of the organic compound.

In terms of thermodynamics, the reduction power of electrons in semiconductors is dependent on the energy level of the conduction-edge layer. In contrast, the capacity of the edge layer is a measure of the strength of the oxidizing holes in semiconductors. Different semiconductors have different band gap edges. A layer edge with a higher potential capacity corresponds with increased oxidizing intensity of the holes [27]. In order to have complete photocatalytic activity towards a variety of organic molecules, the band layer should have a relatively high potential. Semiconductors with a small energy gap more efficiently absorb the sunlight. Therefore, semiconductors with small energy gaps are better for the utilization of sunlight. Selection of a semiconductor photocatalyst depends on the optimization of factors including oxidation power, overlap with the solar spectrum, and photochemical and chemical stability. Titanium dioxide has good chemical and photochemical stability. However, its applications as a catalyst are limited by its poor overlap with the solar spectrum [27]. This study investigates

doping TiO₂ to resolve this problem, as doping decreases the energy gap and brings the wavelength of absorption from the UV range into the visible range.

4. SUMMARY

Fe-doped TiO₂ nanoparticles were successfully synthesized by the sol-gel method. Properties of Fe-TiO₂ nanoparticles differ from those of TiO₂ nanoparticles, including smaller particle size and extension of light absorption towards the visible region. Doping TiO₂ with Fe induces a shift in the energy band gap to a lower energy, i.e., from 3.2 to 2.5 eV for pure TiO₂ and Fe-TiO₂ nanoparticles, respectively. These experiments revealed that Fe-TiO₂ induces a more effective photocatalytic oxidation of furfural than TiO₂. A 95% degradation of furfural was observed using Fe-TiO₂/UV in comparison to 76% using Fe-TiO₂/sun.

ACKNOWLEDGEMENTS

The authors express their thanks to the laboratory staff of the Department of Environmental Health Engineering, Faculty of Health and Health Sciences of the Mazandaran University of Medical Sciences, Sari, Iran for their collaboration, and to the Research Deputy of Mazandaran University of Medical Sciences for the financial support of this study (Project No. 92-1).

REFERENCES

- [1] SINGH S., SRIVASTAVA V.C., MAL I.D., *Fixed-bed study for adsorptive removal of furfural by activated carbon*, Colloids Surf., A., 2009, 322 (1), 50.
- [2] ANBIA M., MOHAMMADI N., *A nanoporous adsorbent for removal of furfural from aqueous solutions*, Desalination, 2009, 249 (1), 150.
- [3] ANBIA M., MOHAMMADI N., *Heterogeneous photocatalytic degradation of furfural using NiS-clinoptilolite zeolite*, Desalination, 2011, 273 (1), 248.
- [4] MESGARI Z., GHARAGOZLOU M., KHOSRAVI A., GHARANJIG K., *Spectrophotometric studies of visible light induced photocatalytic degradation of methyl orange using phthalocyanine-modified Fe doped TiO₂ nanocrystals*, Spectrochim. Acta, Part A., 2012, 92, 148.
- [5] MURDOCH M., WATERHOUSE G.I.N., NADEEM M.A., METSON J.B., KEANE M.A., HOWE R.F., LLORCA J., IDRIS H., *The effect of gold loading and particle size on photocatalytic hydrogen production from ethanol over Au/TiO₂ nanoparticles*, Nat. Chem., 2011, 3 (6), 489.
- [6] MILLS G., HOFFMANN M.R., *Photocatalytic degradation of pentachlorophenol on titanium dioxide particles: identification of intermediates and mechanism of reaction*, Environ. Sci. Technol., 1993, 27 (8), 1681.
- [7] PEARSON A., JANI H., KALANTAR-ZADEH K., BHARGAVA S.K., BANSAL V., *Gold nanoparticle-decorated Keggin ions/TiO₂ Photocatalyst for improved solar light photocatalysis*, Langmuir, 2011, 27 (11), 6661.
- [8] GIRGINOV C., STEFICHEV P., VITANOV P., DIKOV H., *Silver doped TiO₂ photocatalyst for methyl orange degradation*, J. Eng. Sci. Technol. Rev., 2012, 5 (4), 14.
- [9] LI F.B., LI X.Z., HOU M.F., *Photocatalytic degradation of 2-mercaptobenzothiazole in aqueous La³⁺-TiO₂ suspension for odor control*, Appl. Catal., B., 2004, 48 (3), 185.

- [10] PEARSON A., ZHENG H., KALANTAR-ZADEH K., BHARGAVA S.K., BANSAL V., *Decoration of TiO₂ nanotubes with metal nanoparticles using polyoxometalate as a UV-Switchable reducing agent for enhanced visible and solar light photocatalysis*, *Langmuir*, 2012, 28 (40), 14470.
- [11] PRIMO A., CORMA A., GARCIA H., *Titania supported gold nanoparticles as photocatalyst*, *Phys. Chem. Chem. Phys.*, 2011, 13 (3), 886.
- [12] BORGHEI S., HOSSEINI S., *Comparison of furfural degradation by different photooxidation methods*, *Chem. Eng. J.*, 2008, 139 (3), 482.
- [13] FARAMARZPOUR, M., VOSSOUGH M., BORGHEIA M., *Photocatalytic degradation of furfural by titania nanoparticles in a floating-bed photoreactor*, *Chem. Eng. J.*, 2009, 146 (1), 79.
- [14] CHEN L., ZHU J., LIU Y.-M., CAO Y., LI H.-X., HE H.-Y., DAI W.-L., FAN K.-N., *Photocatalytic activity of epoxide sol-gel derived titania transformed into nanocrystalline aerogel powders by supercritical drying*, *J. Mol. Catal. A, Chem.*, 2006, 255 (1–2), 260.
- [15] YU S., YUN H.J., LEE D.M., YI J., *Preparation and characterization of Fe-doped TiO₂ nanoparticles as a support for a high performance CO oxidation catalyst*, *J. Mater. Chem. A.*, 2012, 25 (22), 12629.
- [16] ASL S.K., SADRNEZHAAD S.K., KEYANPOUR RAD M., UNER D., *Comparative photodecolorization of red dye by anatase, rutile (TiO₂), and wurtzite (ZnO) using response surface methodology*, *Turk. J. Chem.*, 2012, 36, 121.
- [17] WANG, X., WU Z., WANG Y., WANG W., WANG X., BU Y., ZHAO J., *Adsorption-photodegradation of humic acid in water by using ZnO coupled TiO₂/bamboo charcoal under visible light irradiation*, *J. Hazard. Mater.*, 2013, 262, 16.
- [18] SAHU A., SRIVASTAVA V.C., MALL I.D., LATAYE D.H., *Adsorption of furfural from aqueous solution onto activated carbon. Kinetic, equilibrium and thermodynamic study*, *Sep. Sci. Technol.*, 2008, 43 (5), 1239.
- [19] CHIOU C.-H., JUANG R.-S., *Photocatalytic degradation of phenol in aqueous solutions by Pr-doped TiO₂ nanoparticles*, *J. Hazard. Mater.*, 2007, 149 (1), 1.
- [20] JAMIL T.S., GHALY M.Y., FATHY N.A., ABD EL-HALIM T.A., ÖSTERLUND L., *Enhancement of TiO₂ behavior on photocatalytic oxidation of Mo dye using TiO₂/AC under visible irradiation and sunlight radiation*, *Sep. Sci. Technol.*, 2012, 98, 270.
- [21] ZHANG M., JUAN W., JIAN H., JIANJUN Y., *Molybdenum and Nitrogen Co-Doped Titanium Dioxide Nanotube Arrays with Enhanced Visible Light Photocatalytic Activity*, *Sci. Adv. Mater.*, 2013, 5 (6), 535.
- [22] KHAN M.M., ANSARI S.A., PRADHAN D., ANSARI M.O., HAN D.H., LEE J., CHO M.H., *Band gap engineered TiO₂ nanoparticles for visible light induced photoelectrochemical and photocatalytic studies*, *J. Mater. Chem. A.*, 2014, 2 (3), 637.
- [23] ZAZOULI M.A., EBRAHIMZADEH M.A., YAZDANI-CHARATI J., SHIRALIZADEH DEZFOLEI A., ROSTAMALI E., VEISI F., *Effect of sunlight and ultraviolet radiation in the titanium dioxide nanoparticle for removal of furfural from water*, *J. Mazandran. Univ. Med. Sci.*, 2013, 23 (107), 139 (in Persian).
- [24] PONGWAN P., INCEESUNGVORN P., WETCHAKUN K., PHANICHPHANT S., WETCHAKUN N., *Highly efficient visible-light-induced photocatalytic activity of Fe-doped TiO₂ nanoparticles*, *Eng. J.*, 2012, 16 (3), 143.
- [25] KIM M.-S., RYU C.S., KIM B.-W., *Effect of ferric ion added on photodegradation ofalachlor in the presence of TiO₂ and UV radiation*, *Water Res.*, 2005, 39 (4), 252.
- [26] PANG Y.L., ABDULLAH A.Z., *Effect of low Fe³⁺ doping on characteristics, sonocatalytic activity and reusability of TiO₂ nanotubes catalysts for removal of Rhodamine B from water*, *J. Hazard. Mater.*, 2012, 235–236, 326.
- [27] CHEN X., MAO S.S., *Titanium dioxide nanomaterials. Synthesis, properties, modifications, and applications*, *Chem. Rev.*, 2007, 107 (7), 2891.